Ultra-small footprint silica-on-silicon WDM based on Holographic Bragg Reflectors

D. Iazikov, C. Greiner*, and T. W. Mossberg
LightSmyth Technologies, Inc., 860 W. Park St., Ste 250, Eugene, OR 97041

ABSTRACT

We report on wavelength-division-multiplexing (WDM) based on lithographically-fabricated slab-waveguide-contained planar holographic Bragg reflectors (HBRs). Partial HBR diffractive contour writing and contour displacement are successfully demonstrated to enable precise bandpass engineering of multiplexer transfer functions and make possible compact-footprint devices based on hologram overlay. Four and eight channel multiplexers with channel spacings of ~ 50 and ~100 GHz, improved sidelobe suppression and flat-top passbands are demonstrated. When a second-order apodization effect, comprising effective waveguide refractive index variation with written contour fraction, and the impact of hologram overlap on the hologram reflective amplitude are included in the simulation, excellent agreement between predicted and observed spectral passband profiles is obtained. With demonstrated simulation capability, the ability to fabricate general desired passband profiles becomes tractable.

Keywords: Integrated Optics, Photonic Crystals, Fiber Optics, Distributed Bragg Reflector, Planar Lightwave Circuit, Photonic Bandgap, Apodization, Lithography, Silica-on-Silicon, Holography, Wavelength Division Multiplexing.

1. INTRODUCTION

Planar holographic Bragg reflectors (HBRs) [1-4] are two-dimensional lithographically-scribed volume holograms contained within a planar slab waveguide. In the slab waveguide, optical signals are free to propagate without constraints in two dimensions – a geometry that enables 2D Bragg structures to provide powerful spectral and spatial holographic functions. A single HBR can simultaneously spatially image an input signal to an output port (or from one point within an integrated photonic circuit to another) while at the same time providing spectral filtering of the signal. Unlike fiber and channel-waveguide gratings, where separation of the counter-propagating input and output signals typically requires additional elements, planar HBRs provide spatially distinct and thus easily accessed outputs. HBRs constitute the building blocks of unique integrated photonic circuits that operate entirely without wire-analog channel waveguides, being based on HBR-mediated signal transport where signals freely overlap as they are imaged from active element to active element. The HBR approach marries the power of free-space optics and volume holography with a fully integrated environment. The powerful volume-holographic function provided by HBR structures provides, via computer-generated complex-shaped diffractive contours, fully-optimized spatial mapping of an arbitrary complex input field wavefront to an output field mode tailored to match the chosen output means. This broad *in-plane* spatial wavefront transformation capability contrasts with previously discussed 2D distributed Bragg reflectors intended for *out-of-plane* applications such as laser feedback and outcoupling [5-7] and free-space to slab-waveguide beam coupling [8,9]. HBR spatial wavefront transformation, due to its holographic nature, is generally more powerful than that provided by simple conic section DBRs [10], whose focusing power degrades when input and output optics deviate from the point source limit.

* e-mail: cgreiner@lightsmyth.com; phone: (541)-431-0026; fax: (541)-284-5607

Physics and Simulation of Optoelectronic Devices XII, edited by Marek Osinski, Hiroshi Amano, Fritz Henneberger, Proceedings of SPIE Vol. 5349 (SPIE, Bellingham, WA, 2004) · 0277-786X/04/$15 · doi: 10.1117/12.529695

Recently [3], we demonstrated that photolithographic fabrication of HBRs in silica-on-silicon allows the highly accurate placement of constituent diffractive contours as evidenced by fabrication of fully coherent centimeter-scale planar holographic structures. Additionally, a robust and fabrication-friendly method to control the reflective amplitude of diffractive element contours via partial writing of the latter was presented [4]. Together, precise feature placement and partial contour writing provide control over the phase and amplitude of diffractive elements on an individual line basis. This is enabling to 2D Bragg reflector design for two reasons. *Spectrally*, it offers a pathway to unprecedented precision and flexibility in the design of HBR transfer functions via the tailoring of the diffractive element arrangement. *Spatially*, partial contour writing and displacement allows the overlay of several planar holograms on the same substrate – thus making it possible to design high-resolution (de)multiplexing devices for multi-wavelength signals with very compact footprint. In the present paper, we demonstrate, for the first time, the application of these concepts to the spectral (bandpass) and spatial engineering of multiplexing devices based on holographic Bragg reflectors. We furthermore identify an important coupling between partial contour writing and the effective waveguide index that must be accounted for when using amplitude apodization based on fractional contour writing.

2. RESULTS AND DISCUSSION

Figure 1 is a schematic of a simple four-channel HBR device fabricated to explore the general potential of the HBR approach for spectral multiplexing and to characterize basic device performance. The top view of Figure 1a illustrates the device operational principle. An input signal is coupled into the planar device via an input channel waveguide (IN) from whose endpoint the input beam expands into a slab region. Through interaction with the multiplexer sections in the slab region the input signal is spectrally filtered and spatially directed to one of the four wavelength-specific outputs. The HBR multiplexer consists of four stacked, 5-mm-long holographic Bragg gratings whose vacuum resonance wavelengths, λ_1 through λ_4, increase with distance from the input port in increments of ~0.35 nm, corresponding to about 50 GHz. The precise multiplexer channel spacings and center wavelengths depend on the core thickness and

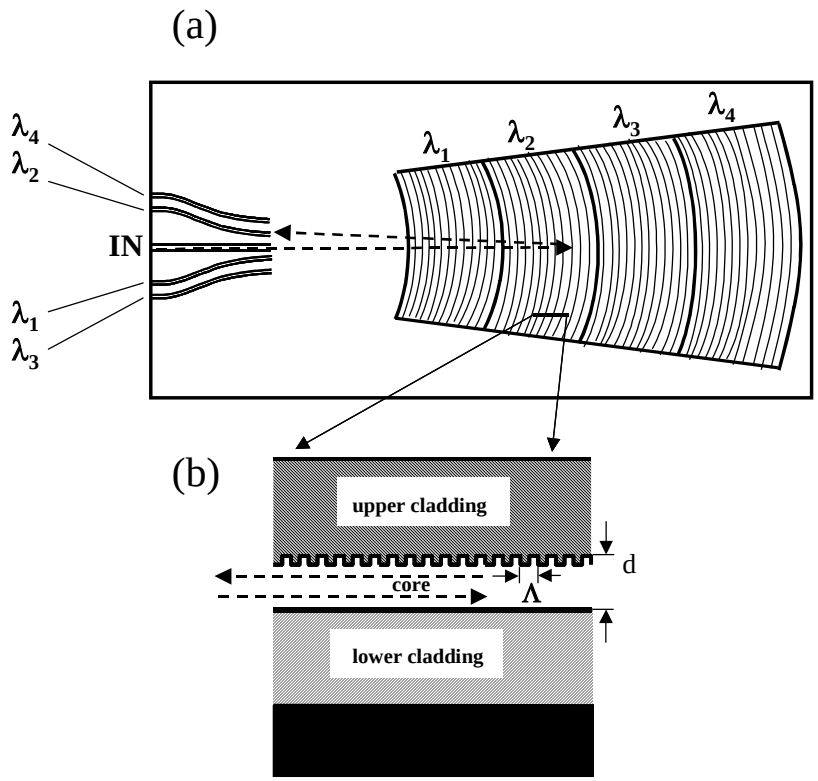


Figure 1. Four-channel wavelength-division multiplexer based on planar holographic Bragg reflectors. 1a, Cross-sectional view; 1b, Top view.

refractive index of the specific waveguide in which the device is lithographically realized. Consistent with our objective to first examine basic device operation and performance no apodization was applied to the grating sections in this initial design. The multiplexer's wavelength-to-output port assignment follows the layout shown in Figure 1a. The HBR diffractive contours, represented in Figure 1a by thin solid lines, can be designed individually to match the back-diffracted input field to the output port. For the devices described here, the diffractive contours were not optimized to provide maximal output coupling. In these early stage devices, contours are configured as circular arcs concentric about the point midway between the end of the input channel waveguide and the beginning of the corresponding output channel waveguide. Fully optimized holographic contours will improve input-output coupling by more effectively coupling to the mode of the output waveguide.

Figure 1b is a partial device cross section. The multiplexers discussed here are based on silica-on-silicon slab waveguides that consist of a central silica core with thickness d = 2 μm or 4 μm and bilateral 15-μm-thick cladding layers. For all the devices, the waveguide core exhibits a + 0.8 % index contrast with respect to its claddings. Also depicted at the upper core-cladding interface are cross-sections of representative lithographically-scribed grating diffractive contours. The diffractive contours, with depth ~450 nm, for all devices, consist of trenches etched into the core and filled with cladding material. All gratings operate in first order with a contour spacing, Λ, of about 500 nm, i.e. one half of the in-medium wavelength of resonant light. In the schematic cross-section of Figure 1b light enters the device from the left side and is coherently backscattered to the left by the diffractive elements.

The multiplexer's input-output channel waveguide manifold (Figure 1a) exhibits an interchannel spacing of 30 μm at the input side to the HBR slab region. Here, all waveguides have a design width of 12.7 μm, adiabatically increased from 6 μm at the die edge via a 1 mm-long taper. The output waveguides are angled with respect to the input waveguide. The angle of a given output waveguide is given by $0.1575°/(30\ \mu m) \times l$, where l is the distance (in microns) between the end point of the input guide and the given output guide. The radius of the HBR's diffractive arc closest to the center of curvature is 3.5 mm. All devices discussed here occupy die areas of only about 1.7 cm^2 including access channel waveguides. All multiplexers reported on in this paper were fabricated from a laser-written reticle employing a DUV optical stepper and standard etching, deposition, and annealing processes.

Figure 2a depicts the designed spectral transfer functions of the four multiplexer channels (band pass profiles). The transfer functions are calculated from the spatial design data using an extensive Fresnel-Huygens diffraction calculation and assuming weak overall device reflectivity. The relatively high adjacent side lobes in the design spectral transfer functions are a direct consequence of the fact that this initial multiplexer design employs grating structures that are unapodized. The adjacent sidelobe suppression seen is essentially dictated by Fourier transform theory. For comparison, the transform-limited sidelobe suppression provided by a uniform grating is shown by the two bars on the right side of Figure 2a. In multiplexer designs discussed below, grating apodization is demonstrated to significantly improve sidelobe suppression. Figure 2b shows the measured spectral transfer functions of the four multiplexer output channels of the fabricated multiplexer for TE-polarized input light. The device was realized in a slab waveguide with d = 4 μm. The results shown in Figure 2b comprise the first successful implementation of a photolithographically-written HBR-based device for spectral multiplexing and indicates an excellent coherent realization of the design structure. The average insertion loss, measured through coupled fibers, was found to be about -3 dB which implies a HBR insertion loss of about -2 dB. Measured channel bandpass functions are broadened and adjacent sidelobes are stronger than seen in the simulation – as expected at the achieved reflectivity levels. The longer wavelength channels (λ_2 - λ_4) are seen to exhibit passband shapes slightly different from the λ_1-channel. These are believed to arise from input depletion caused by signal travel through spatially preceding and partially resonant grating structures. Grating designs incorporating appropriate apodization acting to remove sidelobes of preceding gratings that are spectrally coincident with primary bandpasses of subsequent ones are expected to provide mitigation of this effect.

An inherent advantage of the HBR technology is its capability to address multiplexing needs in a broad range of networks, including those based on hyperfine, dense, and coarse WDM. Specifically, the approach provides for both the ability to implement almost arbitrary channel spacings (both uniform and non-uniform) as well as channel passbands that may be tailored to a very high degree. To demonstrate these properties we have fabricated an eight-channel HBR multiplexer with a channel spacing about twice that of the previous device (i.e., about 100 GHz) wherein channel transfer functions are designed to exhibit

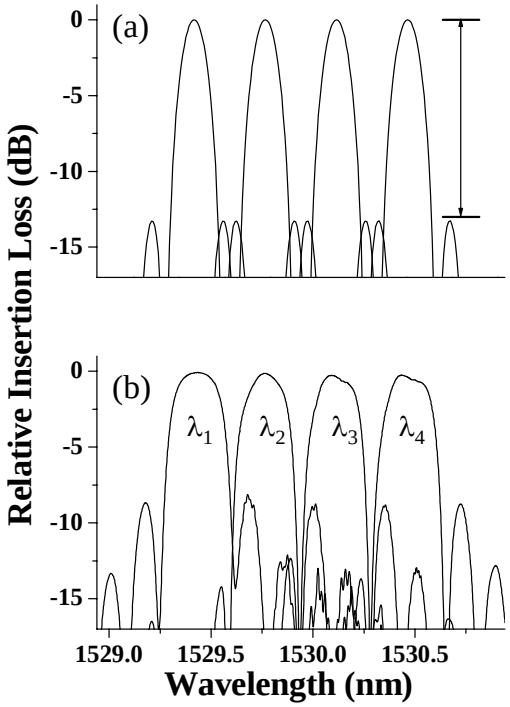


Figure 2. Four-channel multiplexer spectral throughput. 2a, simulated throughput; 2b, Measured response (for TE-polarization). The arrow indicates the transform-limited sidelobe suppression provided by a uniform (unapodized) 1D grating.

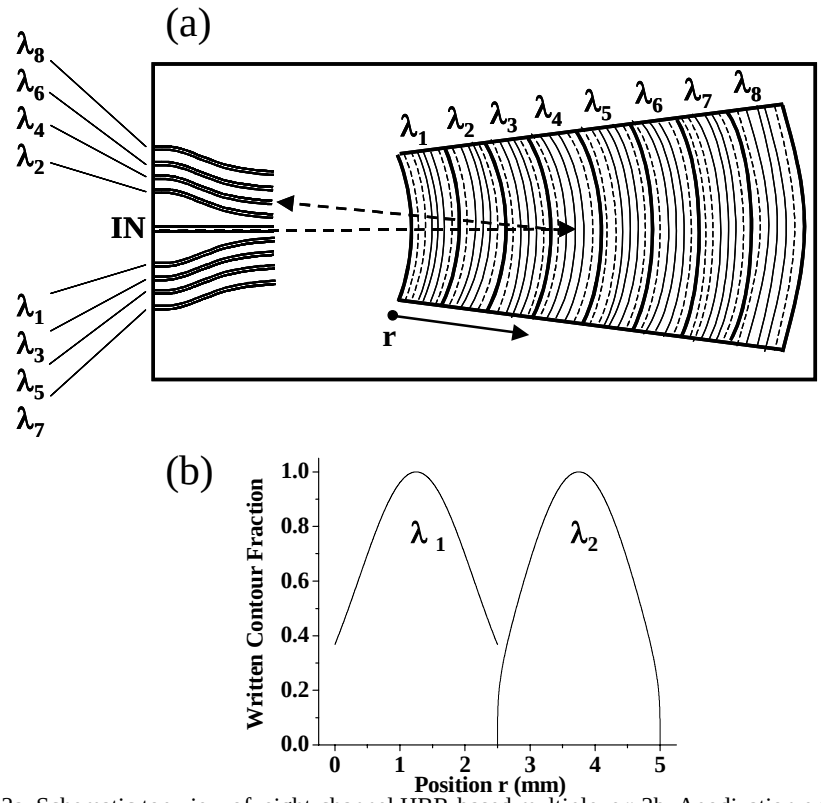


Figure 3. 3a, Schematic top view of eight-channel HBR-based multiplexer; 3b, Apodization profiles for odd (λ_1) and even (λ_2) multiplexer channels.

improved adjacent sidelobe suppression compared to Figure 2. The device layout is shown in Figure 3a.

The multiplexer consists of eight stacked, 2.5-mm-long apodized holographic Bragg gratings. Again, the individual channel-gratings were spatially ordered so that their resonance wavelength increased with distance from the device input side. For the 8-channel multiplexer of Figure 3a, d = 4 μm. Engineering of the multiplexer's bandpass employs the fact that the grating spectral transfer function is determined by the detailed contour spacing and relative reflective amplitude of the diffractive contours as a function of position along the input direction. Specifically, in the limit of weak device reflectivity, the transfer function is proportional to the spatial Fourier transform of the amplitude distribution of diffracted light along that direction [1]. In the devices of concern here, diffractive contour amplitude and phase apodization is achieved via partial contour writing and positional displacements, respectively [4]. Two different, amplitude-only adpodization profiles, shown in Figure 3b, and based on the partial-fill method were employed in the device of Figure 3a. All gratings with an even (odd) channel number are designed with the apodization function used for the λ_1- (λ_2) channel. All parameters of the access waveguide manifold of the device shown in Figure 3a are the same as for the device of Figure 1a.

Figure 4a depicts the designed spectral transfer function of the eight multiplexer channels. Note the improved suppression (> 20dB) of sidelobes immediately adjacent to the main channel passband compared to that evident in the designed bandpass of the unapodized four-channel device of Figure 2a. Figure 4b gives the measured spectral transfer function of the eight channels of the fabricated device for TE-polarized input light. Agreement between measured and designed performance is good except for the unexpectedly high side lobes on the long wavelength side of each primary passband. The device average intrinsic insertion loss (due to weak reflection) was found to be about -7 dB. The long-wavelength sidelobes in the measured multiplexer response are found to arise from a second-order apodization effect, detailed below,

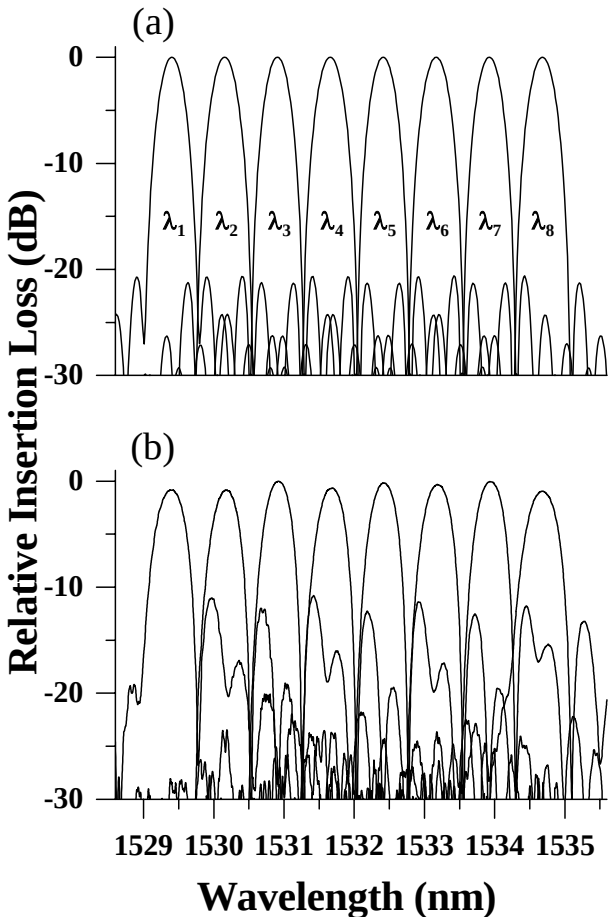


Figure 4. Eight-channel multiplexer spectral throughput (core thickness d = 4 μm). 4a, Multiplexer design spectral transfer function, simulated with constant refractive index; 4b, Measured spectral response (for TE-polarization).

that was unaccounted for in the device designs. The second-order effect comprises an effective refractive index variation inadvertently introduced by using partial contour fill to effect amplitude apodization. Note that the spectral transfer functions of the channels to the very left (λ_1) and right (λ_8) in Figure 4b are seen to exhibit slightly higher insertion losses and broader bandpasses than all other channels of the same respective apodization function. This effect was caused by a photolithographic fabrication error wherein 10% (20%) of the originally designed length of the λ_1- (λ_8) grating was not written.

In the present multiplexer design, apodization of the reflective amplitude of HBR diffractive contours is achieved through partial contour writing [4]. Nominally continuous diffractive contours are written fractionally, with the written contour fraction determining the contour's reflective amplitude. Contour writing occurs through etching (and filling with cladding material) of trenches into the core. Variations in the written trench fraction due to amplitude apodization lead to differences in waveguide morphology that cause variations in the slab waveguide effective refractive index and consequently the Bragg resonance condition. Measurements performed on various test grating structures, each having diffractive contours of fixed written fraction, show a small and approximately linear variation of effective waveguide refractive index with written trench fraction. The fractional effective index difference between a waveguide without a grating and one with a Bragg reflector employing fully written, first-order trenches was found to be - 2 ×

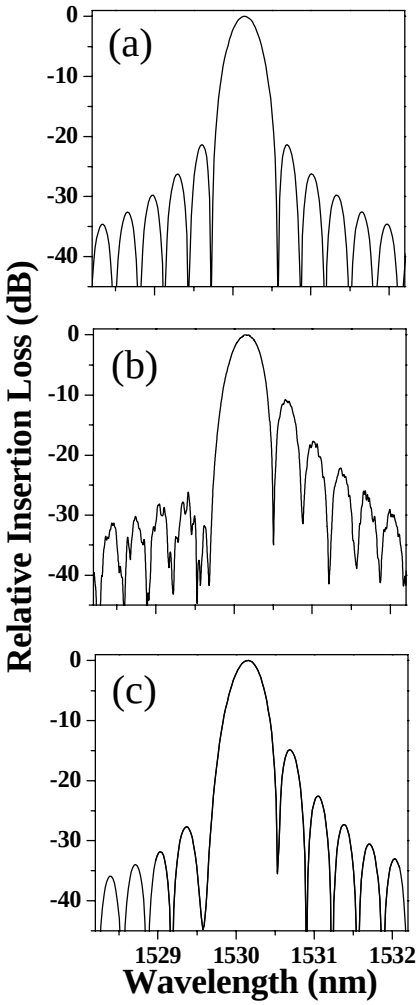


Figure 5. Detail of the passband function for the second multiplexer channel (λ_2). 5a, Simulated throughput, calculated with constant effective index; 5b, Measured throughput (for TE-polarization); 5c, Simulated throughput, calculated with account for apodization-induced effective index changes.

10^{-4} with slab waveguide core thickness d = 4 μm and ~450 nm deep diffractive trenches.

In Figure 5 we explore the impact of the apodization-induced resonance shifts on the multiplexer spectral transfer function. Figure 5a is a blow up of the original design passband function for the second multiplexer channel (λ_2) calculated with constant effective slab waveguide refractive index. Figure 5b shows the detailed measured spectral response for the same channel. Figure 5c shows the passband profile simulated including the effect of measured apodization-induced effective refractive index changes. A comparison of Figures 5b and 5c shows that the simulation now clearly reproduces all features of the fabricated device. The center wavelengths of the simulations (Figure 5a and 5c) were adjusted to coincide with the measured center wavelength (Fig 5b) to facilitate comparison.

Lithographically-enabled partial writing (amplitude apodization) and displacement (phase shifts) of contours not only makes possible the precise bandpass engineering of multiplexer spectral transfer functions but also enables the overlay of planar holograms [1] on the same substrate providing for very compact footprint devices. We apply this concept to the design of a 4-channel ~100 GHz channel-spacing HBR-based multiplexer with designed flat-top channel passbands. Figure 6a is a top view schematic of an overlain HBR device. The device comprises apodized individual-channel HBRs that are staggered along the input beam direction but are heavily overlapping as well. Each hologram is realized with a maximum written trench fraction of 0.65 which ensures that the aggregate (summed over all holograms) written trench fraction at any given position in the multiplexer does not exceed unity significantly (< 1.1). The multiplexer is based on a 2-μm thick slab waveguide. Parameters of the input/output waveguide manifold are the same as for the device of Figure 1. Figure 6b depicts the apodization profile of the λ_1 – channel. Negative portions in the apodization function correspond to π phase shifts of the reflected field and were realized by spatially offsetting the diffractive contours of the corresponding grating sections by λ/4 spatial

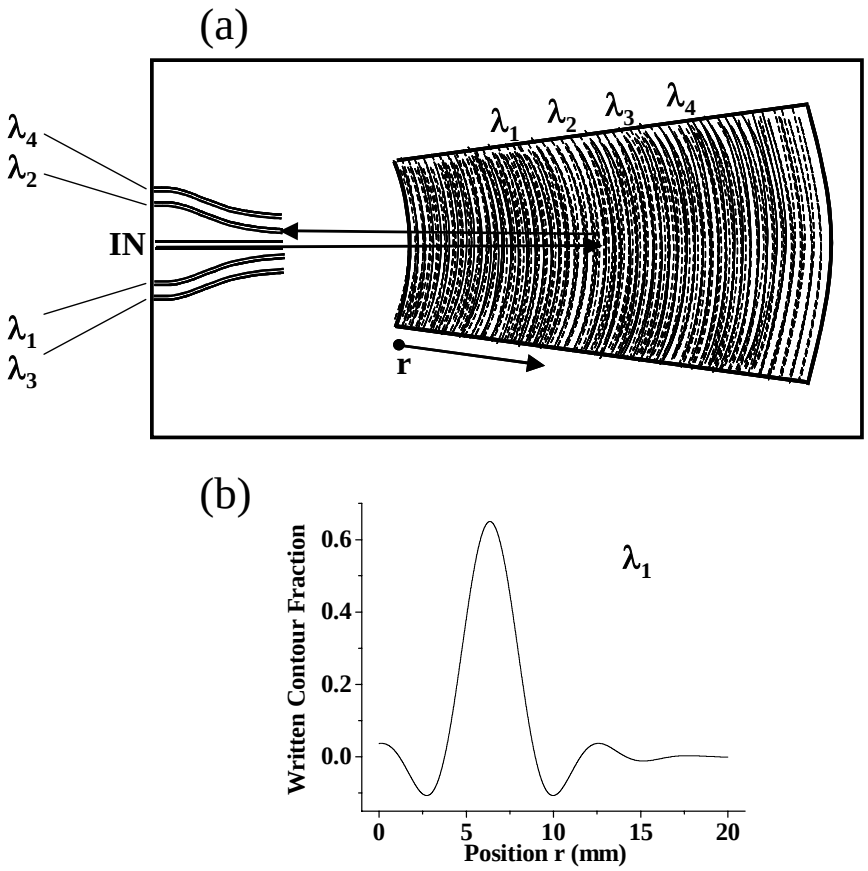


Figure 6. 6a, Schematic top view of four-channel flat-top HBR-based multiplexer based on overlaid planar holograms; 6b, Apodization profile for leftmost (λ_1) multiplexer channel.

shifts with respect to the positive grating sections.

Figure 7a (7b) depicts the simulated (measured) spectral transfer functions of the various multiplexer channels for TE-polarized input light. The measured passbands clearly show the designed flat passband and channel spacing. The multiplexer's adjacent channel isolation exceeds -22 dB. This is excellent for a first iteration design. The absolute multiplexer insertion loss through coupled fibers was about -6 dB implying a -5 dB device intrinsic loss, primarily caused by low device reflection. Discrepancies between measured and designed channel transfer functions such as the long-wavelength shoulder of the measurement arise principally from two factors. First, apodization-induced effective index changes are not compensated for in the present multiplexer design. Second, in designing the device, the various individual-channel HBRs were overlaid without taking detailed precaution to avoid overlap of diffractive contours belonging to different holograms. Due to the present constant-etch-depth multiplexer layout, the overall device reflective strength at a given position is not a linear sum of all contributing diffractive contours at that location. Rather, portions of a given hologram that coincide with diffractive contours of a different grating exhibit a reflective amplitude that is reduced from its design value. Consequently, the actual apodization of a planar hologram is altered from the original design value through two position-dependent effects, i.e. (1) variations in slab waveguide effective refractive index and (2) variations in expected reflective amplitude. Both effects must be accounted for to correctly predict the bandpass function of the fabricated multiplexers. Consideration of these same effects at the design stage allows for precisely crafted bandpass engineering.

Figure 8 explores the impact of the above described phenomena on the spectral transfer function of the λ_1 multiplexer channel. Figure 8a is a blow up of the original design passband function calculated with constant effective index and without account for the reduction of reflective amplitude caused by hologram overlap. Figure 8b shows the detailed measured TE-polarized spectral response for the same channel.

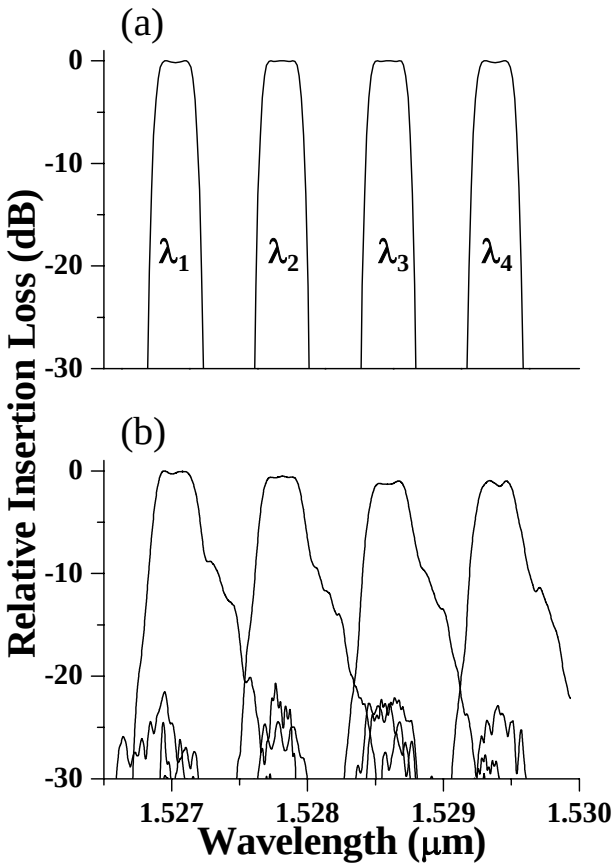


Figure 7. 7a, Multiplexer spectral transfer function simulated with constant effective index; 7b, Measured multiplexer spectral transfer function (for TE-polarization).

Figure 8c shows the passband profile simulated with both the spatially varying effective refractive index and reflective amplitude changes accounted for as described below.

The apodization and overlap effects lead to a position-dependent effective waveguide refractive index which we model as

$$n_{eff}(r) = n_o(1 - 6\times10^{-4}(1 - R(r)),$$

where *R(r)* is the unetched (no written trenches) fraction of slab waveguide at each position, *r,* within the device and n_o is the effective index of the slab waveguide in the absence the HBR contours. *R(r)* was calculated according to

$$R(r) = \prod_{i=1}^{N}(1 - a_i \times G_i(r)),$$

where $G_i(r)$ is the written diffractive contour fraction of the ith planar grating at position *r* and α_i is its duty cycle. The summation runs over all HBRs written. In the present multiplexer design all gratings operate in the first grating order, thus $\alpha_i = 0.5$ for i = 1,…, N.

The reflective amplitude of the jth planar hologram as modified by grating superimposition is written as

$$A_j(r) = A_j'(r)\prod_{i=1,i\neq j}^{N}(1 - \alpha_i \times G_i(r)),$$

where $A_j'(r)$ is the apodization function that pertains in the absence of overlap. The sum runs over all HBRs except for the jth. As comparison of Figures 8b and 8c shows the simulation now clearly reproduces all features of the fabricated device. The simulated passbands shown in Figure 8 were adjusted to exhibit coincident center wavelengths to facilitate straight-forward profile comparison. Overall, the results shown in Figure 7 and 8 demonstrate both the feasibility of spectral passband engineering and the ability to construct devices based on overlaid HBRs.

The agreement between the simulation of Fig. 8c and the measured bandpass spectrum of Fig. 8b is quite excellent. It is apparent from this agreement that the photolithographic fabrication method employed reproduced the design set of grating elements with great precision. The multiplexers studied here were designed without consideration of the effective refractive index variation with amplitude apodization and the impact of hologram overlay on reflective amplitude. Multiplexer designs can be simply corrected for the effect of apodization-induced effective refractive index changes by scaling the separation between grating lines to keep optical path distances constant. Overlay-induced reflective amplitude reduction may be avoided by employing higher grating orders or lower peak fill fractions and implementing a design algorithm wherein spatially overlapping contour elements are displaced to avoid overlap. Alternatively, overlap effects may simply be added to the design algorithm. It should be noted that the HBR overlap multiplicity is constrained by the required reflective strength. For fixed diffractive contour index contrast and waveguide dimensional parameters the net reflective strength per unit surface area is subject to constraints. Evaluation of the details of these constraints is beyond the scope of the present work, but it appears that overlay has advantages over spatial stacking when, for example, spectral resolution necessitates structures that extend spatially beyond the device length required to obtain adequate reflectivity. In this case, overlay of spatially extended but locally weakly reflecting (low partial fill) structures can provide a pathway to high-resolution multiplexers in an overall footprint that is smaller than that necessitated by spatially separated HBR structures.

The measurements shown in this work employ TE-polarized input signals. For TM-input polarization, the grating bandpass functions were observed to shift by approximately +0.65 nm (+0.72 nm) for devices with a core thickness d = 2 μm (d = 4 μm). Measurements of other HBR devices have indicated that polarization-dependent wavelength shifts originate from residual slab wave guide birefringence [3]. No (about 0.3 dB of) polarization-dependent loss (PDL) was measured for multiplexers implemented in the 4-μm (2-μm) thick slab waveguides. For d = 2 μm, the observed PDL is consistent with magnitudes expected to arise from access channel waveguides, either through propagation loss or fiber-to-waveguide coupling.

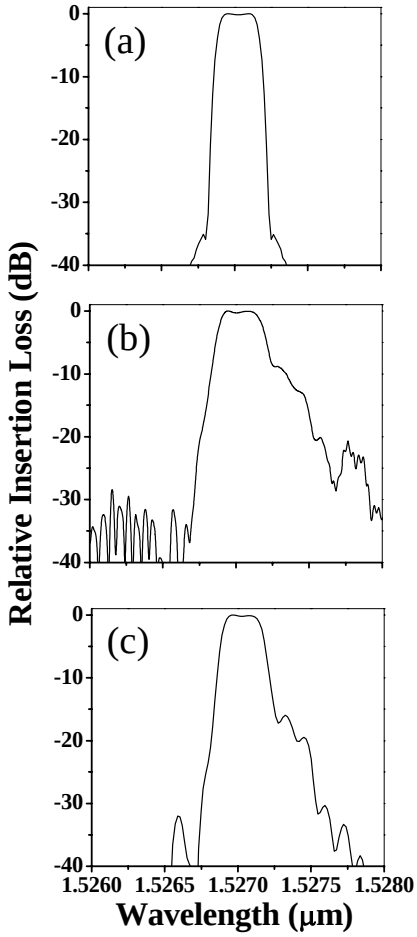


Figure 8. Blow-up of the leftmost multiplexer channel. 8a, Constant effective index simulation; 8b, Measured passband; 8c, Multiplexer throughput calculated including apodization-induced effective index variations and reflective amplitude reduction due to hologram overlay.

This was corroborated by independent measurement of the latter. In the limit of strong grating reflectivity, the reflective bandwidth ratio for TE and TM polarization, γ, is directly proportional to that of the TE and TM amplitude reflection coefficients and can be used to estimate the latter. From test results for $d = 2$, we find $\gamma = 1.018$. Based on this value we estimate the weak-reflectivity ($R \approx 10\%$) PDL inherent to the HBR to be about 0.15 dB and correspondingly less for more strongly reflecting devices as is the case with the muliplexers reported on here.

As constructed, the present HBR-based multiplexers operate at low to moderate reflectivity. Detailed calculations, to be presented elsewhere [11], indicate that achievable alterations in diffractive structure geometry and refractive-index contrast will lead to HBRs of centimeter-scale having strong reflectivity and thus low insertion loss over an aggregate bandwidth as large as several hundred nanometers, i.e. broad enough to support a 16-channel CWDM multiplexer with 13-nm-wide flat-top passbands. Furthermore, a wide range of HBR internal designs is possible providing even broader reflection bands and fully consistent with low loss at the fiber-to-die interface. It appears entirely feasible to integrate much of the functionality currently attributed to discrete-component based thin-film filters into the fully integrated environment. We note also that waveguide-sampled HBR structures [4] offer a pathway to mitigation of polarization dependent wavelength shifts.

III. CONCLUSIONS

In summary, we have demonstrated the viability of planar holographic Bragg reflectors as powerful building blocks for wavelength-division multiplexers. Our present results demonstrate, for the first time, 1) the application of the simultaneous spectral and spatial processing capability of photolithographically-written HBR structures to spectral multiplexing, 2), the successful bandpass engineering of HBR-based multiplexers via fractional writing and positional displacements of constituent diffractive contours and 3), the spatial overlay of multiple HBR structures to create high resolution multiport integrated photonic devices of compact footprint. From a more general point of view, the powerful spectral and spatial beam control inherent to the planar volume-holographic approach offers the possibility of channel-waveguide-free integrated photonic circuits wherein signal routing and processing occurs entirely through interaction with distributed diffractive structures like the HBR. Furthermore, as planar surface-relief structures, HBRs promise consistency with low-cost, mass-production, nanoreplication techniques such as hot embossing or nanoimprint lithography. In embossed/stamped formats, HBR's present an economic route to volume production of high performance optical communications components for datacom and access networks.

REFERENCES

1. T. W. Mossberg, "Planar holographic optical processing devices", Opt. Lett. 26, 414-416 (2001).
2. T. W. Mossberg, "Lithographic holography in planar waveguides", SPIE Holography Newsletter 2, 1 and 8 (2001).
3. C. Greiner, D. Iazikov, and T. W. Mossberg, "Lithographically-fabricated planar holographic Bragg reflectors", J. Lightwave Technol., accepted for publication.
4. D. Iazikov, C. Greiner, and T. W. Mossberg, "Effective gray-scale in lithographically-scribed planar holographic Bragg reflectors", Appl. Opt., accepted for publication.
5. T. Erdogan and D. G. Hall, "Circularly symmetric distributed feedback laser: coupled mode treatment of TE vector fields," J. Quant. Electron. 28, 612-623 (1992).
6. R. H. Jordan, D. G. Hall, O. King, G. Wicks, and S. Rishton, "Lasing behavior of circular grating surface emitting semiconductor lasers," J. Opt. Soc. Am. B 14, 449-453 (1997).
7. S. Kristjansson, N. Eriksson, A. Larsson, R. S. Penner, and M. Fallahi, "Observation of stable cylindrical modes in electrically pumped circular grating-coupled surface-emitting lasers," Appl. Opt. 39, 1946-1953 (2000).
8. M. Li, B. S. Luo, C. P. Grover, Y. Feng, and H. C. Liu, "Waveguide grating coupler with a tailored spectral response based on a computer-generated waveguide hologram," Opt. Lett. 24, 655-657 (1999).
9. J. Backlund, J. Bengtsson, C. Carlstrom, and A. Larsson, "Input waveguide grating couplers designed for a desired wavelength and polarization response," Appl. Opt. 41, 2818-2825 (2002).
10. C. H. Henry, R. F. Kazarinov, Y. Shani, R. C. Kistler, V. Pol, and K. J. Orlowsky, "Four-channel wavelength division multiplexers and bandpass filters based on elliptical Bragg reflectors", J. Lightwave Technol. 8, 748-755 (1990).
11. D. Iazikov, C. Greiner, and T. W. Mossberg, "Apodizable integrated filters for coarse WDM and FTTH-type applications", submitted to J. Lightwave Technol..

Copyright 2004. Society of Photo-Optical Instrumentation Engineers (SPIE). This paper was published in the Proceedings of SPIE, Vol. 5349-32, January 2004, pp. 236-247, and is made available as an electronic reprint with permissionof SPIE. One print or copy may be made for personal use only. systematic or multiple reproduction, distribution, duplication of any material in this paper for a fee or for commercial purposes or modification of the content of the paper are prohibited.